AMERICAN SCIENTIFIC PUBLISHERS

Science of Advanced Materials
Vol. 6, pp. 1–12, 2014
(www.aspbs.com/sam)

ARTICLE

Green Synthesis of ZSM-5 Zeolite Prepared by Hydrothermal Treatment of Perlite. Effect of Chemical Composition and Characterization of the Product

Pablo F. Corregidor*, Delicia E. Acosta, and Hugo A. Destéfanis

Facultad de Ingeniería, Instituto de Investigaciones Para la Industria Química—INIQUI—Universidad Nacional de Salta (UNSa)—CONICET, Consejo de Investigaciones de la UNSa (CIUNSa), Av. Bolivia 5150, A4408FVYA Salta, Argentina

ABSTRACT

We studied the influence of the chemical composition of the starting synthesis gel (SiO_2/Al_2O_3, H_2O/SiO_2, amount of seed and pH) on the preparation of ZSM-5 zeolite by hydrothermal treatment of expanded perlite. Gels with molar compositions of $SiO_2/Al_2O_3 = 20–55$ and $H_2O/SiO_2 = 25–45$, formed at pH values varying from 10.1 to 10.5, produced ZSM-5 zeolite, crystallizing at 453 K for 24 h in a seeded system. Compared with the conventional autoclave treatment, this method avoids the use of environmental-toxic organic structure directing agents. The highly crystalline ZSM-5 zeolite obtained was characterized employing a variety of analytical techniques, including X-ray powder diffraction, scanning electron microscopy, nitrogen adsorption-desorption isotherms, Fourier transform infrared spectroscopy (FTIR), infrared studies of pyridine sorption, ^{27}Al MAS NMR, ^{29}Si MAS NMR and thermogravimetric analysis. At pH values of 13.0 and 13.3, the MFI phase changed to Phillipsite and Analcime, with intermediate formation of amorphous phase at pH 12.0, rearranging the 5–5–1 elements into S4R and S6R units. It was found that the use of an amorphous and low-cost silicoaluminate as starting material can lead, through an inexpensive methodology, to a highly valuable microporous material with many potential applications.

KEYWORDS: Molecular Sieves, Zeolites, ZSM-5, Expanded Perlite, Hydrothermal Treatment.

1. INTRODUCTION

Many years ago, ecological problems posed the need for studying new materials, among which zeolites attracted research interest mainly due to their new and unique properties and their significant worldwide occurrence. Thus, an objective during the last decades was to extend further the possibilities of the preparation methods of zeolites and/or to optimize the synthesis of existing ones. Therefore, the methodology has been modified in the search for: (1) lowering the cost of the procedures that yield each type of zeolite and (2) protecting the environment, thus avoiding the use of environmental-toxic agents. Today, synthetic zeolites are used commercially more often than natural ones due to the purity of crystalline products and the uniformity of particle sizes. The main advantages of synthetic zeolites, in comparison with naturally occurring ones, are that they can be engineered with a wide variety of chemical properties and pore sizes, and also that they exhibit greater thermal stability. Synthetic zeolites can be produced from a variety of natural silica-rich materials including acidic volcanic glasses;[1] among them, natural and expanded perlite are attractive raw materials due to their high content of both silica and alumina. Perlite is a rhyolitic glass made up of more than 70% of silica and 13% of alumina, by weight; it occurs in various types and forms depending on the location of formation. There have been reports on the conversion of perlite to zeolitic materials such as zeolite A and X,[2] phillipsite and sodalite,[3,4] ZSM-5,[5] and Y-zeolite,[6] revealing a novel way of enhancing the commercial value of the mineral. Although the synthesis of zeolites from volcanic glasses provides opportunities for upgrading mineral resources that are either not exploited or utilized in other industrial applications,[6] it usually yields zeolitic products with variable purity.[7] During the last years, the main problem in zeolite research has been the availability and cost of raw materials, especially of silica sources. On the other hand, commercial

*Author to whom correspondence should be addressed.
Email: pcorregidor@unsa.edu.ar
Received: xx xx xxxx
Accepted: xx xx xxxx

ARTICLE

silica (made of sand), which is available in gel, sol, fumed or amorphous solid forms, has been found to have variable reactivity and selectivity. Yet, cheaper raw materials such as clay minerals, natural zeolites, coal ashes, municipal solid waste incineration ashes, volcanic glasses and industrial slags, are used as starting materials for zeolite synthesis.

Zeolites are usually synthesized by hydrothermal procedures using aqueous clear solutions and organic templates, which are required to form a microporous structure. The microporosity of zeolites is frequently caused by the incorporation of pore-generating species such as alkylammonium ion, which compensate negative charges in the crystallizing silicate framework;[8] one of the most commonly used for the preparation of ZSM-5 zeolite is tetrapropyl ammonium ion (TPA^+). The use of an organic template suffers from several significant drawbacks. First, the as-obtained crystals contain organic template in their void spaces, and for many applications the template has to be removed, which is often achieved by calcination, leading to irreversible aggregation. Second, the use of a template in the synthesis tends to change the Si/Al ratio of the final products, which could drastically affect their applicability. Third, the organic templates involved in the syntheses are very expensive, and their use can be environmentally unfriendly.

Numerous studies have been carried out on the synthesis of ZSM-5 zeolite without[9–11] and with different template agents,[12–14] as well as with different sources of materials.[15–17] The effect of synthesis conditions on crystal morphology and reaction time were studied by some researchers.[9, 13, 14]

Starting with Grose and Flanigen, there have been many studies on the crystallization of ZSM-5 zeolite from TPA^+-free reaction mixtures.[9, 14, 18–26] However, in contrast with the case of TPA^+-containing systems, the crystallization of ZSM-5 zeolite from TPA^+-free batches often occurs within relatively narrow ranges of SiO_2/Al_2O_3 and Na_2O/SiO_2. The batches with compositions outside of these ranges often yield impurity phases, such as unreacted amorphous solids,[19] quartz,[18] mordenite[20] or analcime.[24] These disadvantages generate unsatisfactory results in the synthesis of ZSM-5 zeolite without organic templates.[9, 19] However, these difficulties can be overcome by the addition of small amounts of seed crystals to the TPA^+-free reaction mixture,[18, 23, 27] which results in the formation of a ZSM-5 zeolite with a high degree of crystallinity and a narrow size distribution at short synthesis times.[18]

Ren et al.[28] proposed a mechanism for the seeded crystallization of ZSM-5 by analyzing the influence of alkalinity on the structural, particulate and chemical properties of the crystalline end products obtained by hydrothermal treatment. They proposed that crystallization can be defined by a chain of processes starting with:
(i) dissolution of the amorphous silica and/or aluminum source, followed by
(ii) formation of (alumino) silicate gel by polycondensation reactions (a part of the gel is deposited onto the surfaces of seed crystals, forming an amorphous shell around them);
(iii) formation of 5-1 secondary building units and their condensation into active growth precursor species in the matrix gel;
(iv) deposition of the growth precursor particles from the amorphous shell onto the surfaces of seed crystals;
(v) "ordering" of the deposited growth precursor particles by their gradual transformation from an amorphous and/or partially crystalline phase to a fully crystalline phase (zeolite ZSM-5).

It is well known that seed-assisted methods have opened the door to produce low-cost and environmentally-friendly zeolites in industry but, to the best of our knowledge, only a few reports investigate the synthesis of ZSM-5 zeolite from expanded perlite in the absence of an organic template; we thus think that greater knowledge and a better understanding must be acquired concerning this field. Therefore, the aim of this work was to study the synthesis of zeolites from a low-cost silica–alumina source such as Argentinian perlite by changing the chemical composition of the synthesis gel expressed as SiO_2/Al_2O_3, H_2O/SiO_2, amount of seed and pH values, with the expectation of obtaining ZSM-5 with the highest percent of crystallinity. Finally, the results of the synthesis and the properties of the material were subsequently evaluated by different characterization techniques.

2. EXPERIMENTAL DETAILS

2.1. Materials

Expanded perlite from San Antonio de los Cobres (Northwestern Argentina) was previously conditioned by washing with water, followed by grinding and sieving with a 230 mesh sieve before using as starting material. In order to obtain the appropriate SiO_2/Al_2O_3 molar ratio in the synthesis gel, sodium silicate (Fisher; Na_2O 27.7 wt% with a SiO_2/Na_2O ratio of 2:1 approximately) was used as additional Si source. A sodium form of a commercial ZSM-5 zeolite (ALSI-Penta SN-55, $SiO_2/Al_2O_3 = 23$) was used as a crystallization seed.

2.2. Synthesis of ZSM-5

In the present study, the chemical composition of the initial system was optimized for the preparation of ZSM-5 zeolite, using a seed of 7 wt% of the total silica amount in the initial gel. After mixing the reactants, the mixture was allowed to age at room temperature for a few hours and then treated hydrothermally at 453 K for 24 h. Organic-free ZSM-5 synthesis was performed with the composition $SiO_2/Al_2O_3 = 20–55$ and $H_2O/SiO_2 = 25–45$, conducted at various pH values ranging from 10.1 to 13.3. Expanded perlite was used as the only Al source and sodium silicate was employed as a supplementary Si source to obtain

the optimum Si/Al molar ratio. The hydrothermal synthesis of ZSM-5 was performed in 20 mL Teflon-lined stainless steel-autoclaves using H_2SO_4 or NaOH aqueous solution to adjust the pH and the Na_2O/SiO_2 molar ratio of the reaction mixture. After completion of the reaction, the autoclaves were cooled at room temperature, the product was centrifuged at 2000 r.p.m. for 5 minutes; the solid was washed with distilled water until the pH of the supernatant reached the value of 7–8, and finally dried at 393 K overnight. Zeolites obtained in the Na^+ form of ZSM-5 were previously converted to the NH_4-ZSM-5 form by ion-exchange with a 10 wt% solution of NH_4Cl at 353 K.[29] At the end, the NH_4^+ form was converted to the H-ZSM-5 form by heating under air flow at 723 K overnight for further characterization.

2.3. Characterization

The powder X-ray diffraction (XRD) patterns were recorded on a STOE STADI P instrument using CuKα radiation ($\lambda = 0.15415$ nm) to identify the product phase and to calculate the percentage of crystallinity. Diffraction lines of 2θ between 5° and 45° were taken to confirm the phase of ZSM-5 zeolite, and the degree of crystallinity was calculated by comparing the sum of the areas below the dominant peaks between 22° and 25° 2θ of each sample with the sum of the areas above the reference ZSM-5 sample (ALSI-Penta SN-55, $SiO_2/Al_2O_3 = 23$).

The specific surface area and the porosity characteristics were determined from N_2 adsorption/desorption isotherms using the multipoint BET method. The samples were outgassed under 1.0×10^{-6} mbar vacuum at 623 K for 10 h prior to the measurements, and isotherms were obtained at liquid nitrogen temperature with a Quantachrome Quadrasorb SI automated gas adsorption system. The external surface area and the micropore volume were determined from the adsorption branch of the isotherm using the *t*-plot method.

Crystal morphology and size were identified by Scanning Electron Microscopy (SEM) with a JEOL JSM-6480 LV microscope at an operating voltage of 15. Before measurement, all the samples were treated with gold sputtering.

The aluminum coordination state of the zeolite samples was confirmed by ^{27}Al magic angle spinning nuclear magnetic resonance (^{27}Al MAS NMR). The spectra were recorded on a Bruker Advance DSX400 spectrometer operating at a magnetic field strength of 9.4 T; 36000 scans were accumulated with a spinning frequency of 20 kHz, a pulse length of 0.3 μs and a recycle delay of 100 ms. The ^{27}Al signals were referenced to an externally located 0.1 mol$\cdot$L^{-1} aqueous solution of $[Al(H_2O)_6]^{3+}$. ^{29}Si magic angle spinning nuclear magnetic resonance spectra (^{29}Si MAS NMR) were recorded by accumulating 4000 scans with a spinning frequency of 5 kHz, a pulse width of 5 μs and a pulse delay of 60 s on a Bruker AMX300 spectrometer working at 7.0 T. Tetramethylsilane was used as a chemical shift reference.

Fourier transform mid-infrared (FT-IR) spectra were recorded on a Perkin Elmer FT-IR Spectrum GX instrument using KBr pellets (approximately 1 wt% zeolite in a KBr matrix), in the range of 400–4000 cm^{-1}.

Thermogravimetric analysis (TGA) was conducted under nitrogen gas with a TGA analyzer (TA Instrument) to study the thermal stability of the material. The synthesized sample was subjected to a heating rate of 10 degrees$\cdot$min^{-1}, from room temperature to 1173 K.

The strength and distribution of acid sites were tested by adsorption and programmed desorption of pyridine using infrared (IR) spectroscopy. The infrared spectra of zeolite samples were recorded in a Nicolet 6700 spectrometer equipped with a DTGS detector (128 scans, 2 cm^{-1} resolution). A self-supporting wafer (of about 15 mg) of the sample was evacuated in a homemade vacuum infrared cell fitted with ZnSe windows. The wafer was dried at 673 K for 1 h under vacuum. During the cooling down of the sample, reference spectra were recorded at 623, 523, 423 and 323 K. The evacuated sample was saturated with about 25 mbar of pyridine vapor at 323 K. The saturated wafer was then evacuated at 323 K for 30 min and temperature-programmed desorption of adsorbed amine was carried out at a heating rate of 5 degrees$\cdot$min^{-1}, maintaining the temperature at 423, 523 and 623 K for 30 min. The infrared spectra of adsorbed pyridine were recorded at these temperatures. The corresponding reference spectra were subtracted from these spectra and the band intensities at wavenumbers 1540 and 1450 cm^{-1} were determined and assigned to bands of Brønsted and Lewis acid sites of adsorbed pyridine, respectively. The concentration of Brønsted and Lewis acid sites was calculated with the integral molar extinction coefficients of pyridine infrared absorption bands determined by Emeis.[30]

3. RESULTS AND DISCUSSION

3.1. Characterization of Expanded Perlite

Perlite is a volcanic glass that is able to expand 4–20 times of its original volume when heated rapidly at 923–1473 K, resulting in a particular structure of flakes with high porosity. Perlite consists mainly of the following oxides, expressed as weight percentages: SiO_2, 73.36%; Al_2O_3, 13.49%; Na_2O, 3.42% and 4.84% of K_2O. However, the SiO_2/Al_2O_3 molar ratio in expanded perlite is too low to synthesize the highly siliceous ZSM-5 zeolite. The X-ray powder diffraction pattern in Figure 1 revealed that the solid composition of expanded perlite was amorphous in nature. The BET surface area was 2 m$^2\cdot$g^{-1} (Table III) while the SEM micrographs in Figure 4(a) showed a highly porous sponge-like material with a smooth thin surface and a randomly fragmented structure, as a result of the expansion process.[31] Perlite morphology was

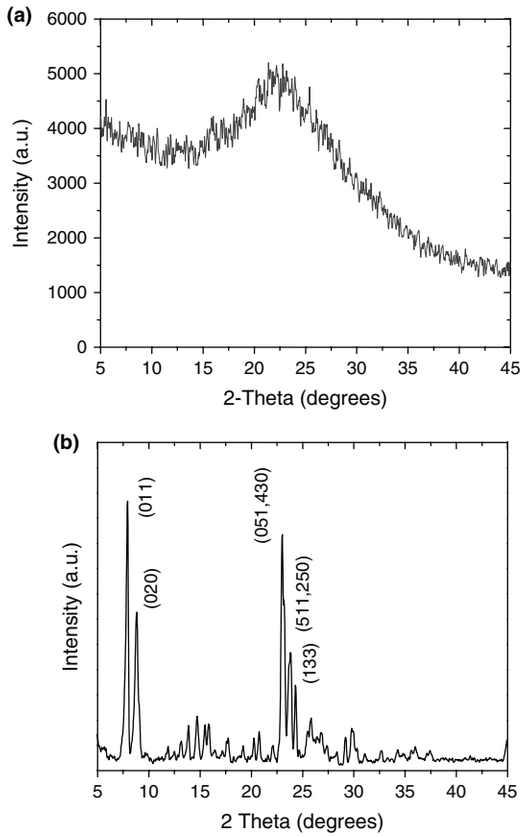

Fig. 1. XRD powder pattern. (a) Expanded perlite and (b) Na-ZSM-5 obtained from hydrothermal treatment of perlite under optimum conditions (for the references to optimum conditions, the reader is referred to the text of this article).

characterized by the presence of individual flakes with smooth surface and thickness.

3.1.1. Effect of the Composition in the Reaction Mixture

In this study, ZSM-5 zeolite with different degrees of crystallinity and other zeolite phases were obtained by varying the synthesis conditions, as will be discussed in detail later in this article. The most probable mechanistic pathways in zeolite formation are briefly described in chronological sequence as induction period, nucleation, and crystal growth.[8, 28, 32]

It is commonly known that silicon–aluminum zeolites are formed by the polymerization of silicon and aluminum species from a strongly basic solution under specific temperature and autogenous pressure. The conditions for the transformation of the inexpensive Argentinian perlite to zeolite are shown in Table I. The influence of SiO_2/Al_2O_3, H_2O/SiO_2, amount of seed and pH in the starting synthesis gel was evaluated by determining the crystallinity of the obtained phase at a reaction time of 24 h at 453 K and by varying one operational condition while keeping other factors unchanged.

Table I. Crystallization field for hydrothermal treatments of perlite at 453 K and 24 h, varying the chemical composition of the initial gel, expressed as SiO_2/Al_2O_3, H_2O/SiO_2 and pH. We used (a) 0.0700 g of crystallization seed and (b) a 7% wt seed/SiO_2.

SiO_2/Al_2O_3	H_2O/SiO_2	pH	Seed	Crystallinity (%)	Products
20[a]	23.75	10.2	0.0700 g	6	ZSM-5
25[a]	23.75	10.2	0.0700 g	23	ZSM-5
31[a]	23.75	10.2	0.0700 g	43	ZSM-5
35[a]	23.75	10.2	0.0700 g	76	ZSM-5
40[a]	23.75	10.2	0.0700 g	90	ZSM-5
45[a]	23.75	10.2	0.0700 g	84	ZSM-5
55[a]	23.75	10.2	0.0700 g	70	ZSM-5
40[b]	25	10.2	7%	21	ZSM-5
40[b]	30	10.2	7%	51	ZSM-5
40[b]	35	10.2	7%	70	ZSM-5
40[b]	40	10.2	7%	84	ZSM-5
40[b]	45	10.2	7%	94	ZSM-5
40[b]	45	10.1	7%	94	ZSM-5
40[b]	45	10.2	7%	94	ZSM-5
40[b]	45	10.3	7%	94	ZSM-5
40[b]	45	10.4	7%	94	ZSM-5
40[b]	45	10.5	7%	93	ZSM-5
40[b]	45	10.8	7%	72	ZSM-5
40[b]	45	11.3	7%	< 5	ZSM-5
40[b]	45	12.0	7%	n.a.	Amorphous
40[b]	45	13.0	7%	n.d.	Phillipsite
40[b]	45	13.3	7%	n.d.	Analcime
40[b]	45	10.2	1%	49	ZSM-5
40[b]	45	10.2	3%	65	ZSM-5
40[b]	45	10.2	5%	76	ZSM-5
40[b]	45	10.2	7%	94	ZSM-5
40[b]	45	10.2	9%	78	ZSM-5

Notes: n.d. = not determined; n.a. = not applicable.

3.1.2. Effect of the SiO_2/Al_2O_3 Molar Ratio

Without addition of sodium silicate, the SiO_2/Al_2O_3 molar ratio in expanded perlite is 9.2. In order to obtain SiO_2/Al_2O_3 molar ratios of 20, 25, 31, 35, 40, 45 and 55, expanded perlite was mixed with adequate amounts of sodium silicate without altering the H_2O/SiO_2 molar ratio, the amount of seed and the pH of the mixture. The latter was controlled at 10.2 ± 0.1 by adding small amounts of H_2SO_4 or NaOH solutions. In order to show clearly the possible region in which pure ZSM-5 is formed, the crystallization field of the phases obtained from the starting gel is shown in Table I.

Maintaining all synthesis parameters unchanged and increasing the SiO_2/Al_2O_3 ratio from 20 to 25, no coffin-shaped particles were detected, but smaller fragments of particulate material (compared with the initial one) were present due to the alkaline hydrolysis of flakes and sponge-like fragments of expanded perlite (Figs. 2(a) and (b)). The formation of incipient small coffin-shaped particles was evident at a SiO_2/Al_2O_3 molar ratio of 35 (Fig. 2(c)). Increasing the SiO_2/Al_2O_3 values from 31 to 35 results in an increase of particle sizes from $\sim$500 nm to $\sim$700 nm, the latter having well delimited borders and a more defined coffin-like shape (Fig. 2(d)).

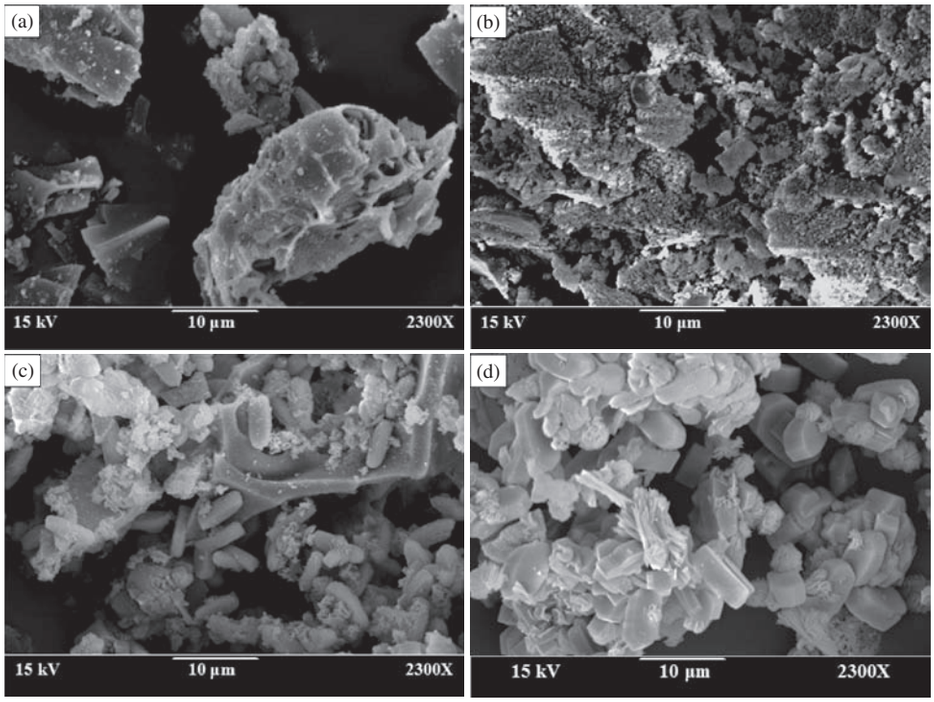

Fig. 2. SEM microphotographs of the products obtained at SiO_2/Al_2O_3 mole ratios of: (a) 20, (b) 25, (c) 31 and (d) 35.

From the analysis of XRD powder patterns (not shown) it was found that only ZSM-5 zeolite can be synthesized at SiO_2/Al_2O_3 molar ratios from 20 to 55. ZSM-5 zeolite formed at SiO_2/Al_2O_3 ratios above 20, and it was confirmed that the concentration of silica was sufficient for the supersaturation of Si species and suitable for the formation of a ZSM-5 phase. The crystallinity of ZSM-5 zeolites, obtained from XRD patterns, is shown in Table I. A maximum of 90 wt% crystallinity was found at a SiO_2/Al_2O_3 molar ratio of 40. Since this crystallinity of the ZSM-5 zeolite was optimal for the monitored range, it was then used in the following experiments.

3.1.3. Effect of the H_2O/SiO_2 Molar Ratio

Water is always used as solvent for hydrothermal synthesis of zeolite materials. In the hydrothermal system, it often acts as

(i) space filler,
(ii) hydrolyser and reformer of the M—O—M bond (where M and O denote metal and oxygen atoms, respectively),
(iii) accelerator of chemical reactions, and
(iv) viscosity-maintaining agent.[33]

All these non-solvent characteristics of water are believed to influence the nucleation and crystal growth of zeolite materials. The effect of water content in the starting gel was therefore studied for optimizing the preparation of ZSM-5.

The H_2O/SiO_2 molar ratio of the batch was adjusted from 25 to 45 in the gel with composition $40SiO_2 \cdot Al_2O_3 \cdot 0.38Na_2O \cdot yH_2O$ by varying the y value from 1000 to 1800 under the conditions shown in Table I. The crystallization field of the synthesis gels with different water content levels clearly shows that the lower the water content in the mixture, the lower the crystallization percent of the ZSM-5 phase. Although this effect is in contrast with the general principle that dilution of the crystallizing system causes a decrease of the concentration of reactive species in the liquid phase, and thus a reduction of the crystal growth rate,[34, 35] the observed increase of crystal growth (Fig. 3) when increasing the H_2O/SiO_2 molar ratio is probably related to the relatively high SiO_2 concentrations in the studied system, where most of the silica is probably present in colloidal form. Since colloidal silica negligibly affects growth behavior, the formation of the primary building units by depolymerization of colloidal silica in the diluted systems may cause an increase in the growth of ZSM-5.

3.1.4. Effect of the pH Value

Alkalinity is one of the most important parameters for controlling the crystallization in the synthesis of zeolites. In the absence of organic species, hydrated sodium cations are able to direct the MFI structure,[36–38] acting as templates by stabilizing the formation and favoring the assembly of structural subunits to provide the adequate precursors needed for nucleation and crystallization of ZSM-5 zeolite under a specific condition, namely low Na_2O/SiO_2 and

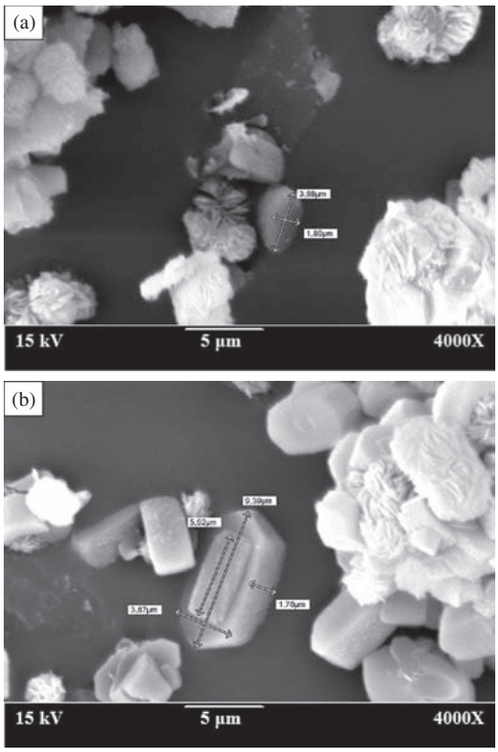

Fig. 3. Scanning electron microscopy images of the products obtained at H_2O/SiO_2 molar ratios of (a) 35 and (b) 40.

high SiO_2/Al_2O_3.[38] For this reason, the synthesis of ZSM-5 from organic template-free reaction mixtures is particularly sensitive to the concentrations of Na^+ and OH^- ions in the reaction mixture. Generally, an increase in alkalinity causes an increase in the crystallization rate via accretion of the crystal growth rate and/or nucleation, consequent to a higher concentration of reactive silicate, aluminate and (alumino) silicate species in the liquid phase of the system.

ZSM-5 zeolite obtained at pH values between 10.1 and 10.5 exhibited a complete crystalline phase and coffin-like particles (Fig. 4(b)), while the morphology was similar to that of conventional MFI-type zeolites.[39] Increasing the alkalinity of the reaction mixture from pH = 10.1 to 10.5 did not increase the crystallinity of the hydrothermal treatment product (Table I), indicating that under given conditions ($10.1 \leq pH \leq 10.5$; $SiO_2/Al_2O_3 = 40$; $H_2O/SiO_2 = 45$; 7% wt of seed; $T = 453$ K and crystallization time of 24 h), only a part of the amorphous (alumino) silicate precursor was used for the formation of ZSM-5 zeolite by the growth of seed crystals.

While the structural properties of the crystallization products were not influenced by the alkalinity of the reaction mixture in the range of $10.1 \leq pH \leq 11.3$, an increase of alkalinity over the upper limit changed both the structural and particulate properties. The structural changes are related to the formation of an amorphous surface layer at pH 12.0 (Fig. 5), followed by the appearance of needle-like particles at pH 13.0 (Fig. 4(d)) which, having diffraction peaks at $2\theta = 12.4°$, 21.7°, 28.1° and 33.5° (Fig. 5), belong to Phillipsite.[40] The appearance of a crystalline phase containing particles with trapezohedral morphology (Figs. 4(e) and (f)) was observed when increasing the pH of the mixture to 13.3, presenting diffraction peaks at $2\theta =$ 15.8°, 18.3°, 25.9°, 30.5°, 33.3° and 35.8° (Fig. 5). These are all characteristics of Analcime zeolite.[41,42] A similar trapezohedral morphology was reported by Atta et al. for Analcime[42] in hydrothermal synthesis using kaolin and rice husk ash.

3.1.5. Effect of Seed Crystals

Seeding is a widely used approach in the large-scale production of zeolites. Nevertheless, the exact mechanism that promotes zeolite crystallization in a seeded system has not been fully understood.[36] Crystal growth of silicalite and ZSM-5 in seeded systems has led to two proposed pathways of crystallization.[43] Ordered growths and subsequently regular overgrowths were reported in sufficiently dilute synthesis mixtures. It was suggested that nucleation took place preferably on the seed crystal surface and that the seed crystal direction controlled the growth of new crystals, causing epitaxial growth. Nucleation in solution dominated in concentrated solutions, and random formations of embedded crystals were observed on seed surfaces. Seed crystals usually lead to new populations of crystals rather than growing themselves to become larger single crystals.

In this work, no synthesis of ZSM-5 zeolite was detected on a non-seeded system under identical conditions of a seeded one until a reaction time of 24 h. As shown in Table I, adding the seed to the reaction mixture helped synthesize ZSM-5; about 7% seeds/SiO_2 was the optimum value in the range of 1–9%. The mentioned range is in excellent agreement with previously reported values by Wang et al.[5]

3.2. Characterization of the ZSM-5 Product Obtained from Expanded Perlite

After synthesis of the material, it is necessary to characterizing it. Appropriate characterization is an indispensable prerequisite for judging the reproducibility of the synthesis as well as its suitability for applications. Knowledge of the characteristics of the as-prepared ZSM-5 (i.e., acidic properties, thermal stability and textural properties) is necessary to understand its possible uses in catalyzed reactions.

3.2.1. XRD Diffraction Pattern

Figure 1(b) shows diffraction patterns with their corresponding *hkl* faces, labeled for the seven most intense peaks of the Na-ZSM-5 zeolite obtained from perlite under optimum conditions. The XRD is in agreement with those already reported elsewhere. Table II shows the crystallographic parameters (lattice parameters and unit cell volume) obtained after applying the auto-indexing method for

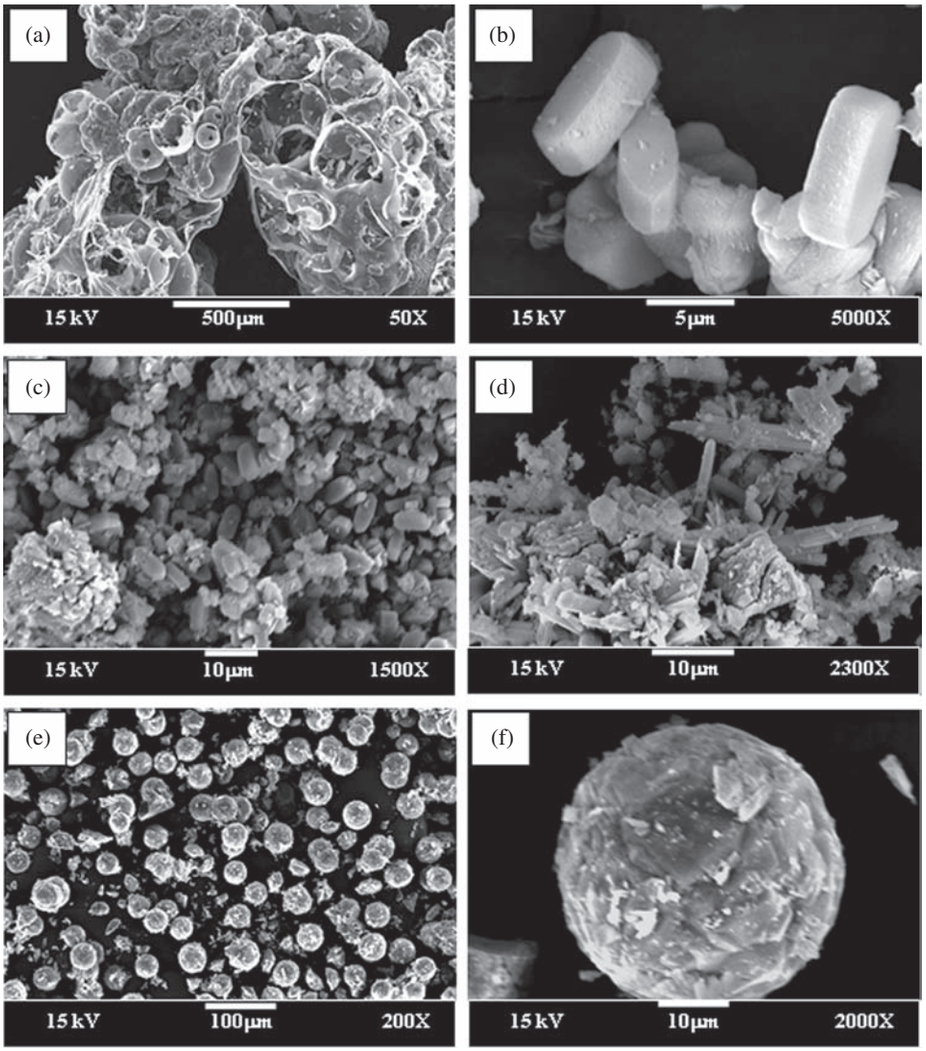

Fig. 4. SEM microphotographs of the expanded perlite submitted to hydrothermal treatment (180 °C) at different pH values. (a) Expanded perlite without any treatment; (b) and (c) pH = 10.2; (d) pH = 13.0; (e) and (f) pH = 13.3.

an orthorhombic cell ($a = 1.9911$ nm, $b = 2.0101$ nm, $c = 1.3367$ nm, $V = 5.3509$ nm^3) using DICVOL 06 software.[44] These results demonstrated that there are no significant changes in lattice parameters (a, b and c) and that they are consistent with the IZA calcined reference,[45] thus validating the rearrangement of the amorphous perlite into a crystalline solid phase that can be characterized as ZSM-5 zeolite.

3.2.2. N_2 Adsorption–Desorption Isotherms

The basic physicochemical and textural properties of expanded perlite and of the as-prepared Na-ZSM-5, determined by Nitrogen adsorption isotherms, are summarized in Table III. Perlite presents a characteristic type II isotherm (Fig. 6), typical of a material that is non-porous or possibly macroporous.

The N_2-adsorption isotherm of the obtained Na-ZSM-5 sample (Fig. 6) is of type I,[46] with an H4 hysteresis loop as defined by IUPAC. A type I isotherm is well defined for micropore adsorbent material without significant mesoporosity, particularly ZSM-5. Nevertheless, an H4 hysteresis loop is usually associated with thin slit-like inter-crystalline pores where the pores are mainly in the micropore range.[47–51] Application of the BET model and the t-plot method confirm that most of the surface area (290 m$^2 \cdot$ g^{-1}) obtained is due to the presence of micropores. Although the validity of the BET model for highly microporous materials is questionable, the surface areas derived from this model in the adapted pressure range of $p/p_0 = 0.01$–0.10 are commonly used for comparative purposes.[52]

The specific surface area (S_{BET}) was obtained by analyzing nitrogen adsorption data at 77 K in a relative vapor pressure range where the value of the BET C constant is positive and the $V \cdot (1 - p/p_0)$ term increases continuously with p/p_0. A total pore volume (V_{tot}) of 0.13 cm$^3 \cdot$ g^{-1}

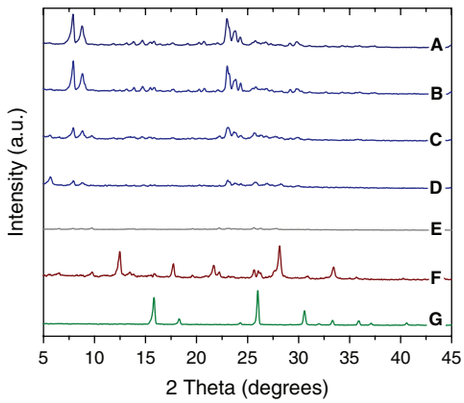

Fig. 5. XRD diffraction pattern of zeolites. (A) Commercial H-ZSM-5 zeolite; (B) to (G) Zeolites obtained from expanded perlite at different pH values: (B) pH = 10.2; (C) pH = 10.8; (D) pH = 11.3; (E) pH = 12.0; (F) pH = 13.0; (G) pH = 13.3.

was estimated by applying the Gurvitch rule based on the volume adsorbed at a relative pressure of 0.99. The micropores, with an average pore diameter of 0.55 nm (Fig. 7) and a volume (V_{mic}) of 0.12 $cm^3 \cdot g^{-1}$, were determined by the Dubinin-Ashtakov equation, while almost the same volume ($V_{mic} = 0.11$ $cm^3 \cdot g^{-1}$) was determined by applying the *t*-plot method (using the Halsey model). These data are comparable and consistent with the data reported in the literature for a ZSM-5 structure. The mesopore volume (V_{Meso}) estimated from V_{tot} and V_{mic} was calculated as 0.01–0.02 $cm^3 \cdot g^{-1}$.

3.2.3. ^{29}Si MAS NMR

The SiO_2/Al_2O_3 ratio of zeolite is thought to be directly related to the thermal, hydrothermal and chemical stability of zeolite materials, as well as to their sorption, acidity and catalytic activity. Therefore, the SiO_2/Al_2O_3 ratio is an imperative characteristic of these materials.

The total silicon concentration is proportional to the total intensity of all five potential resonances in the ^{29}Si spectrum (i.e., $\sum_{n=0}^{4} ISi(OAl)_x$, where $Si(OAl)_x$ represents the local environment $Si(OSi)_{4-x}(OAl)_x$). The total aluminum content is proportional to the weighted sum of all the resonance intensities in the local environments $Si(OSi)_{4-x}(OAl)_x$, where the intensity of each resonance is weighted by the number of aluminum atoms in the local environment. The sum must then be divided by 4 to account for the fact that each silicon atom is connected to four other silicon or aluminum atoms.

According to the Lowenstein's rule,[53] the framework SiO_2/Al_2O_3 molar ratio can be calculated by deconvolution of the ^{29}Si MAS NMR spectra (Gauss model) using Eq. (1):

$$\left(\frac{Si}{Al}\right)_{\text{framework}} = \frac{\sum_{n=0}^{4} I_{Si(nAl)}}{0,25 \sum_{n=0}^{4} n I_{Si(nAl)}} \quad (1)$$

where $I_{Si(nAl)}$ represents the peak area of the Si(nAl) signal in the ^{29}Si MAS NMR spectra and n is the number of AlO_4 groups linked directly with the SiO_4 groups.

The ^{29}Si MAS NMR signal at −112.1 ppm (Fig. 8) was attributed to the resonance of silicon atoms of $Si*(OSi)_4$ groups in the framework of the ZSM-5 structure and overlaps partly with a resonance at approximately −116.4 ppm, attributed to $Si*(OSi)_4$ units due to the presence of crystallographically inequivalent sites in the zeolite. The ^{29}Si MAS NMR spectra also exhibits a broad resonance in a range from −102 to −108 ppm, representing Al–O–$Si*(OSi)_3$ and/or HO–$Si*(OSi)_3$ sites in the ZSM-5 crystals.[54] These findings could confirm the results obtained by textural characterization, indicating that HO–$Si(OSi)_3$ groups could be present in the as-prepared ZSM-5 sample due to some mesoporosity. Moreover, the resonance with chemical shifts at −99.2 ppm is attributed to $(Al–O)_2Si*(OSi)_2$ sites with two Al neighbors.

Based on these results, the ratio of silicon to framework aluminum for the as-prepared Na-ZSM-5 sample was estimated as 38.5.

Table II. Parameters of the crystallographic IZA standards and of the as-prepared Na-ZSM-5 product under optimum conditions.

Sample	Lattice parameters (nm)			Unit cell volume (nm^3)
	a	*b*	*c*	
Na-ZSM-5 (standard IZA calcined)	1.9879	2.0107	1.3369	5.3437
Na-ZSM-5 (standard IZA not calcined)	2.0022	1.9899	1.3383	5.3320
Na-ZSM-5 (from expanded perlite)	1.9911	2.0101	1.3367	5.3509

3.2.4. ^{27}Al MAS NMR

The question that arises when considering the aluminum content of the prepared ZSM-5 zeolite is whether all aluminum was incorporated into the framework. The ^{27}Al spectra show distinct chemical shift ranges for tetrahedral, pentacoordinate, and octahedral environments, and so can be used to distinguish between framework aluminum and extra framework species. Aluminum tetrahedral framework atoms typically resonate at 60–50 ppm, and can be clearly distinguished from five- and six-coordinate extra framework species, which resonate at approximately 25 and 13 to −17 ppm, respectively.[29] The ^{27}Al MAS NMR spectra (Fig. 9) shows a peak at 55 ppm, representative of a tetrahedral environment of aluminum. The absence of a peak at 0 ppm unambiguously proves that all aluminum is incorporated into the framework.[47]

3.2.5. TGA

Figure 10 shows the TGA profile of the Na-ZSM-5 sample in the temperature range of 300–1173 K. The weight loss is due to desorption of water. This TGA pattern, typical of

Table III. Surface area and porosity characteristics of expanded perlite and of the as-prepared Na-ZSM-5 product.

Sample	SiO_2/Al_2O_3 ratio	S_{BET} $m^2 \cdot g^{-1}$	Total pore volume[a], V_{tot} ($cm^3 \cdot g^{-1}$)	Micropore volume, V_{mic} ($cm^3 \cdot g^{-1}$)	Mesopore volume, V_{Mes} ($cm^3 \cdot g^{-1}$)		Average pore diameter, d_p (nm)
				t-plot[b]	D.A. eq[c]	$V_{Mes} = V_{tot} - V_{mic}$	
Expanded perlite	9.2	2	0.05	0.00	0.00	0.05	12.50[d]
Na-ZSM-5	12	290	0.13	0.11	0.12	0.01[b]–0.02[c]	0.55[c]

Notes: [a]At $p/p_0 = 0.99$ (Gurvitch rule); [b]*t*-plot method (Halsey model); [c]Dubinin–Ashtakov equation; [d]Determined by BJH method.

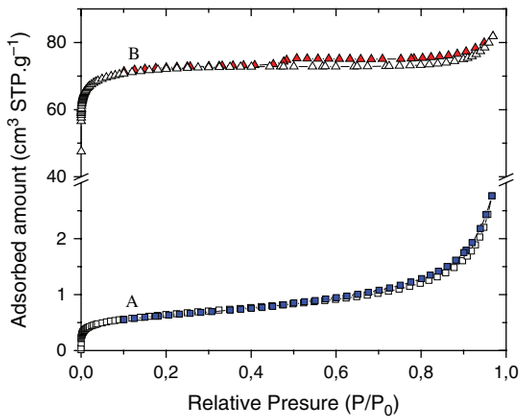

Fig. 6. N_2-adsorption (solid symbols) and desorption (open symbols) isotherms at 77 K of (■) Expanded perlite and (▲) as prepared Na-ZSM-5 sample.

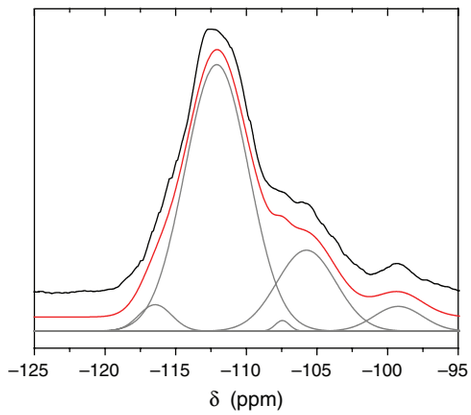

Fig. 8. ^{29}Si MAS NMR of the Na-ZSM-5 product. Experimental spectrum (black), calculated model (red) and Gaussian bands corresponding to the individual resonances (grey).

a ZSM-5 zeolite, shows that the process of water removal is practically complete at ~473 K. The weight loss for the temperature range of 300–523 K, of approximately seven percent in weight, was attributed to water release. It should be mentioned that this is a relatively high water content for a MFI-type material. A small amount of water was still released above 473 K and only for temperatures above 673 K the residual water was completely removed. This indicates that a mild dehydroxylation process took place at high temperatures on the prepared ZSM-5 sample.

3.2.6. FTIR

In the IR spectra, the assignment of bands to ring vibrations can be a basis for determining the type of secondary building units (SBU) and for identifying a given zeolite structure; thus, FTIR will allow us to confirm the different arrangements of the fragments produced when expanded perlite was hydrothermally treated under different alkaline conditions.

The A curve from Figure 11 shows the FT-IR spectra of expanded perlite. The strong band with a maximum

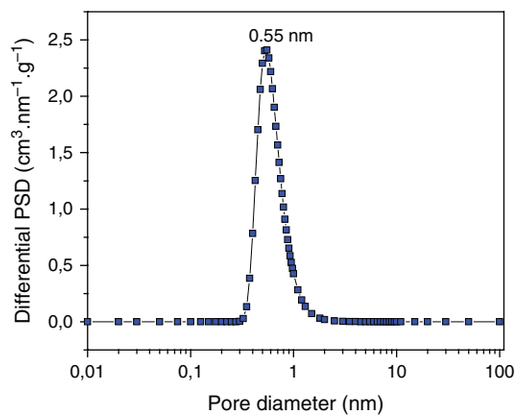

Fig. 7. Differential pore size distribution of the Na-ZSM-5 sample calculated using the Dubinin-Ashtakov method.

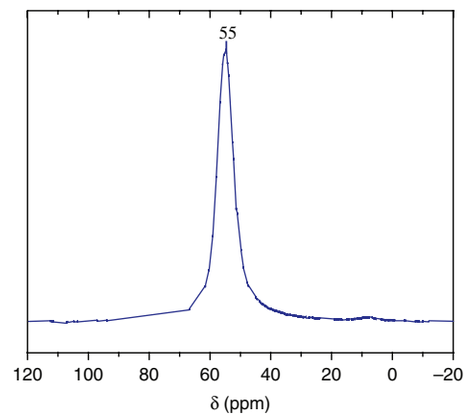

Fig. 9. ^{27}Al MAS NMR of the Na-ZSM-5 product prepared at optimum conditions.

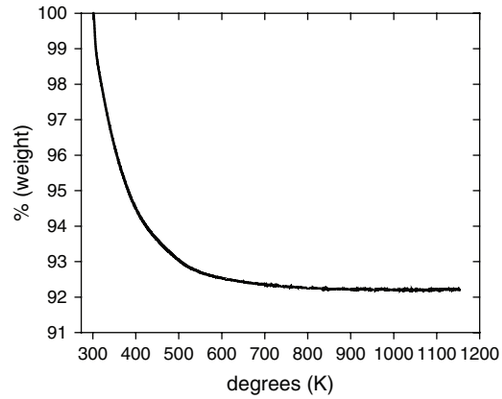

Fig. 10. TGA thermogram of the Na-ZSM-5 sample obtained under optimum conditions.

absorption at 1058 cm^{-1} is usually assigned to the vibration of the Si—O—Si group of the structural siloxane framework due to its amorphous silica content. The strong band at around 1000 cm^{-1} includes the Si—O stretching from $SiO^{-}Na^{+}$ and both Si—O—Si and Si—O—Al asymmetric stretching modes. The region at around 832 cm^{-1} is characteristic of the Si—O—Si symmetric stretching mode in perlite samples.[55] There is also a band that corresponds to the symmetric stretching of the Si—O—Si group at 774 cm^{-1} and a peak at 466 cm^{-1} corresponding to the Si—O—Si and O—Si—O bending modes.

Curves B and C from Figure 11 show FT-IR spectra of commercial and as-prepared Na-ZSM-5 samples, respectively. The bands at 1226–1228 cm^{-1} and 543 cm^{-1} provide information on the differences between ZSM-5 and other zeolite types. The intra-tetrahedral modes corresponding to O—T—O asymmetric stretching at around 1226 cm^{-1} were attributed to the presence of structures

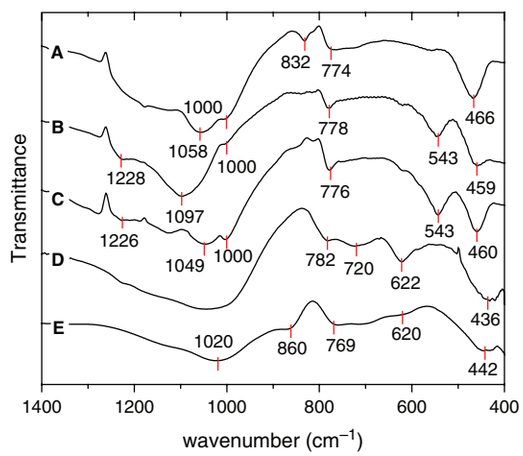

Fig. 11. FTIR spectra. (A) Expanded perlite, (B) commercial Na-ZSM-5, (C) Na-ZSM-5, (D) Phillipsite and (E) Analcime. Samples of (C) to (E) were obtained by hydrothermal treatment of expanded perlite.

containing four chains of 5-membered rings arranged around a two-fold screw axis, as in the case of the ZSM-5 structure.[56] The strong band at 543 cm^{-1} was attributed to the lattice vibration of inter-tetrahedral linkages in the D5R (double five-membered ring).[57] The band around 1049 cm^{-1} was attributed to the intra-tetrahedral mode due to the asymmetric stretching vibration of the Si—O—T linkage.[58] The band near 776–778 cm^{-1} was assigned to the symmetric stretching mode from inter-tetrahedral linkages, while the absorbance at around 460 cm^{-1} was due to the intra-tetrahedral T—O bending vibrations of SiO_4 and AlO_4. The absorption bands around 543 and 457 cm^{-1} are characteristic of the crystalline structure of ZSM-5[59] and the ratio of the intensities of these two peaks provides an estimate of the degree of crystallinity for a given zeolite sample. The ratio of the absorbance of these two bands is 0.7 for the as-synthesized Na-ZSM-5, while the literature suggested a value of 0.8 for a pure ZSM-5 zeolite.[60] This confirms that the as-synthesized ZSM-5 zeolite exhibits good crystallinity, in agreement with the XRD results.

Curve D in Figure 11 exhibits the IR absorption bands of Phillipsite, obtained under the conditions explained before. The bands in the range 720–780 cm^{-1} are characteristic of the S4R group[61,62] of four-membered ring vibrations in which double 8-membered rings are formed by combining S4R units. Bands can occur simultaneously in the same range, at about 780 cm^{-1} and 720 cm^{-1}, due to the vibrations of internal oxygen bridges Si—O—Si and Si—O—Al, respectively. These results and those obtained by XRD are in accordance with the structure of Phillipsite previously proposed.

In Figure 11, curve E shows the FT-IR spectrum of Analcime, obtained under the experimental conditions detailed before. The band at about 860 cm^{-1} is due to the asymmetric stretching of the intra-tetrahedral vibrations of TO_4 tetrahedral units of Analcime, and the one at about 1020 cm^{-1} is due to the asymmetric stretching mode related to intra-tetrahedral linkages. The absorption bands at 769, 620 and 442 cm^{-1} are related to the O—T—O symmetrical stretching mode, the vibrations of 6-membered rings[59,60] and the O—T—O bending vibrations modes,[1] respectively.

Consequently, we can predict a gradual dissolution of the SiO_2 and Al_2O_3 content of expanded perlite under hydrothermal treatment conditions, generating the five-membered ring structures that assemble into a MFI framework at pH values from 10.1 to 11.3. As a result of increasing the concentration of the mineralizing agent, OH^{-} ions tend to dissolve the MFI framework into an amorphous phase at a pH close to 12.0. This re-dissolution produces a rearrangement of the "activated tetrahedral units" into S4R units of the PHI framework at pH = 13.0, and generates the S4R and S6R units of the ANA arrangement at pH values of 13.3.

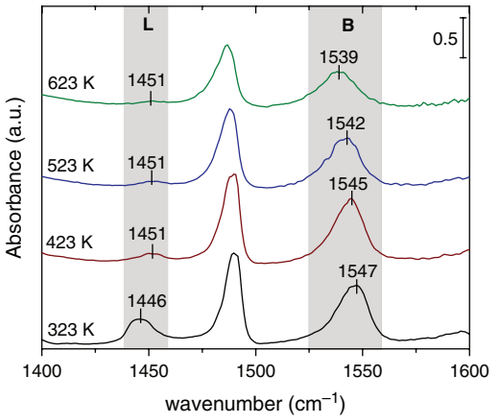

Fig. 12. FTIR spectra of pyridine adsorbed on the as-prepared H-ZSM-5 sample after pyridine desorption at different temperatures: 323, 423, 523 and 623 K.

3.2.7. *Estimation of the Acidic Character Using IR Spectroscopy of Adsorbed Pyridine*

The number of Brønsted and Lewis acid sites were estimated using the integrated molar extinction coefficients (1.67 and 2.22 $cm \cdot \mu mol^{-1}$) determined by Emeis based on the intensities of the infra-red absorption bands found at 1545 cm^{-1} and 1450 cm^{-1}, which correspond to the H-bonding pyridinium ion mode 19b and the coordinatively adsorbed pyridine, respectively.[63–65] The FTIR spectra of the as-prepared H-ZSM-5 sample after desorption of pyridine at four different temperatures is shown in Figure 12. The concentration of Brønsted sites in this sample is 0.30 mmol of py per gram sample, which is close to its framework aluminum content of 0.39 mmol of Al per gram sample. It is clearly shown that the area of the band at about 1545 cm^{-1}, related to Brønsted acid sites, is larger than that of the band at 1450 cm^{-1}. Therefore, the amount of Lewis acid sites is lower than that of Brønsted acid sites; the former is practically negligible compared to the latter. These findings are in line with the presence of only a tetrahedral Al signal in the ^{27}Al MAS NMR spectrum of the as-prepared ZSM-5 zeolite and with a Si/Al molar ratio of 38.5, determined by ^{29}Si MAS NMR.

Table IV. Acidic properties expressed as the number of Brønsted and Lewis sites and percentage of Brønsted acid centers (ΔB), referred to the initial amount at 323 K and saturated with pyridine at given temperature.

Temperature (K)	Brønsted ($mmol \cdot g^{-1}$)	Lewis ($mmol \cdot g^{-1}$)	ΔB^b (%)
323	0.30	n.a.[a]	100
423	0.30	~0	100
523	0.26	~0	87
623	0,21	~0	71

Notes: [a]n.a. = not applicable; [b]ΔB = (Number of Brønsted sites at certain temperature/Number of Brønsted sites at 323 K) × 100.

The Brønsted acid response showed a small variation after heating and a high percent of these acid centers still maintained py bounded, revealing a strong surface acidity (Table IV).

The moderate band observed at 1446 cm^{-1} in the spectra at 323 K should not be confused with the one assigned to Lewis acid sites, as the first practically disappears when temperature increases to 423 K. This behavior should explain the desorption of weakly bounded pyridine due to interactions with silanol groups,[64] which is also in agreement with the presence of the HO–Si(O–Si)$_3$ signal in the ^{29}Si MAS NMR spectra. Therefore, after desorption of pyridine from these weak centers, a band at 1451 cm^{-1} could be observed due to the interactions of very small amounts of the probe molecule with Lewis acid sites.

4. CONCLUSIONS

ZSM-5 zeolite was successfully synthesized by hydrothermal treatment, using expanded perlite as both Si and Al source, by manipulating the chemical conditions in the synthesis. SiO_2/Al_2O_3, H_2O/SiO_2, pH and the amount of seed in the composition of the initial reaction mixture all play an important role in the selective conversion of perlite to a commercially valuable zeolite, determining the type of product and its characteristics. The optimum parameters for a 7% seeded system were a molar composition of $40SiO_2 \cdot 0.38Na_2O \cdot Al_2O_3 \cdot 1800H_2O$, in a pH range of 10.1–10.5, crystallizing at 453 K for 24 hrs. Under the experimental setup used, only ZSM-5 zeolite can be obtained, as long as pH values in the range of $10.5 \leq pH \leq 11.3$ yield small amounts of the zeolite. At higher alkalinity (pH 13.0 and 13.3), the obtained phase changed to Phillipsite and Analcime, respectively, via generation of an amorphous phase at pH 12.0. Therefore, the ZSM-5 framework is a metastable phase that dissolves at high pH values, rearranging the 5-membered rings into S4R and S6R units.

The as-prepared ZSM-5, obtained under optimum conditions, was adequately identified by X-ray diffractometry and solid state FTIR. Scanning electron microscopy, determination of the N_2 adsorption isotherm, ^{29}Si and ^{27}Al MAS NMR, and thermogravimetric analysis, revealed the generation of coffin-shaped particles, a microporous structure, and a Si/Al molar ratio of 38.5 where all the aluminum was in tetrahedral coordination, presenting a stable framework that only releases water upon heating to 1173 K. One of the most important physicochemical characteristics of the material is its density of Brønsted acid sites, maintaining 71% of the adsorbed py at 623 K, thus indicating the presence of centers with a high acidity.

Acknowledgments: The authors gratefully acknowledge the financial support received in the form of a research grant (Program No. 1837) and (Project No. 1837/2) from the Council of Researches of the National

University of Salta (C.I.U.N.Sa.). The authors also would like to thank the laboratory of electronic microscopy (LASEM) of the National University of Salta for the determination of the SEM images.

References and Notes

1. D. W. Breck, Zeolites Molecular Sieves, J. Wiley & Sons, New York (**1974**).
2. N. Giordano, L. Recupero, L. Pino, and J. C. J. Bart, *Ind. Miner.* 83 (**1987**).
3. H. A. Destéfanis, E. Erdmann, and D. E. Acosta, *Int. J. Chem. React. Eng.* 5, 1 (**2007**).
4. A. Rujiwatra, *Mater. Lett.* 58, 2012 (**2004**).
5. P. Wang, B. Shen, and J. Gao, *Catal. Today* 125, 155 (**2007**).
6. G. E. Christidis and H. Papaton, *The Open Miner. J.* 2, 1 (**2008**).
7. D. W. Breck, Industrial Minerals and Rocks, edited by S. J. Lefond, AIME, New York (**1983**), pp. 1399–1413.
8. C. S. Cundy and P. A. Cox, *Chem. Rev.* 103, 663 (**2003**).
9. Y. Cheng, R. H. Liao, J. S. Li, X. Y. Sun, and L. J. Wang, *J. Mater. Process. Technol.* 206, 445 (**2008**).
10. N. Y. Kang, B. S. Song, C. W. Lee, W. C. Choi, K. B. Yoon, and Y. K. Park, *Micropor. Mesopor. Mater.* 118, 361 (**2009**).
11. N. Venkatathri, *Mater. Lett.* 62, 462 (**2008**).
12. C. Falamaki, M. Edrissi, and M. Sohrabi, *Zeolites* 19, 2 (**1997**).
13. O. A. Fouad, R. M. Mohamed, M. S. Hassan, and I. A. Ibrahim, *Catal. Today* 116, 82 (**2006**).
14. S. D. Kim, S. H. Noh, J. W. Park, and W. J. Kim, *Micropor. Mesopor. Mater.* 92, 181 (**2006**).
15. R. Anuwattana, J. Balkus, S. Asavapisit, and P. Khummongkol, *Micropor. Mesopor. Mater.* 111, 260 (**2008**).
16. R. K. Vempati, R. Borade, R. S. Hegde, and S. Komarneni, *Micropor. Mesopor. Mater.* 93, 134 (**2006**).
17. P. Wang, B. Shen, D. Shen, T. Peng, and J. Gao, *Catal. Commun.* 8, 1452 (**2007**).
18. R. Aiello, F. Crea, A. Nastro, and C. Pellegrino, *Zeolites* 7, 549 (**1987**).
19. Y. Cheng, L. J. Wang, J. S. Li, Y. C. Yang, and X. Y. Sun, *Mater. Lett.* 59, 3427 (**2005**).
20. F.-Y. Dai, M. Suzuki, H. Takahashi, and Y. Saito, Zeolite Synthesis, edited by M. L. Occelli and H. E. Robson, American Chemical Society, Washington DC (**1989**), pp. 244–256.
21. H. Kalipcilar and A. Culfaz, *Cryst. Res. Technol.* 36, 1197 (**2001**).
22. R. Lai and G. R. Gavalas, *Micropor. Mesopor. Mater.* 38, 239 (**2000**).
23. M. Lassinantti, F. Jareman, J. Hedlund, and D. Creaser, *J. Sterte, Catal. Today* 67, 109 (**2001**).
24. A. Nastro, F. Crea, D. T. Hayhurst, F. Testa, R. Aiello, and L. Toniolo, Studies in Surface Science and Catalysis, edited by P. A. Jacobs and R. A. van Santen, Elsevier (**1989**), Vol. 49, pp. 321–330.
25. M. Pan and Y. S. Lin, *Micropor. Mesopor. Mater.* 43, 319 (**2001**).
26. N. Ren, Z. J. Yang, X. C. Lv, J. Shi, Y. H. Zhang, and Y. Tang, *Micropor. Mesopor. Mater.* 131, 103 (**2010**).
27. Y. Zheng, X. Su, X. Zhang, W. Wei, and Y. Sun, Studies in Surface Science and Catalysis, edited by A. Sayari and M. Jaroniec, Elsevier, (**2005**), Vol. 156, pp. 205–212.
28. N. Ren, J. Bronic, B. Subotic, X. C. Lv, Z. J. Yang, and Y. Tang, *Micropor. Mesopor. Mater.* 139, 197 (**2011**).
29. K. S. Triantafyllidis, L. Nalbandian, P. N. Trikalitis, A. K. Ladavos, T. Mavromoustakos, and C. P. Nicolaides, *Micropor. Mesopor. Mater.* 75, 89 (**2004**).
30. C. A. Emeis, *J. Catal.* 141, 347 (**1993**).
31. S. N. Hosseini, S. M. Borghei, M. Vossoughi, and N. Taghavinia, *Applied Catalysis B: Environmental* 74, 53 (**2007**).
32. C. S. Cundy and P. A. Cox, *Micropor. Mesopor. Mater.* 82, 1 (**2005**).
33. Y. Hu, C. Liu, Y. Zhang, N. Ren, and Y. Tang, *Micropor. Mesopor. Mater.* 119, 306 (**2009**).
34. S. Bosnar and B. Subotic, *Micropor. Mesopor. Mater.* 28, 483 (**1999**).
35. S. Bosnar, J. Bronic, and B. Subotic, Studies in Surface Science and Catalysis, edited by I. Kiricsi, Elsevier (**1999**), Vol. 125, pp. 69–76.
36. Z. Gabelica, N. Blom, and E. G. Derouane, *Applied Catalysis* 5, 227 (**1983**).
37. P. A. Jacobs and J. A. Martens, Studies in Surface Science and Catalysis, edited by P. A. Jacobs and J. A. Martens, Elsevier (**1987**), Vol. 33, pp. 113–146.
38. J. B. Nagy, P. Bodart, H. Collette, C. Fernandez, Z. Gabelica, A. Nastro, and R. Aiello, *J. Chem. Soc., Faraday Trans.* 1 85, 2749 (**1989**).
39. K. Yamamoto and T. Tatsumi, *Chem. Mater.* 20, 972 (**2007**).
40. M. M. J. Treacy and J. B. Higgins, Collection of Simulated XRD Powder Patterns for Zeolites (fifth), edited by M. M. J. Treacy and J. B. Higgins, Elsevier Science B.V., Amsterdam (**2007**), pp. 342–343.
41. A. Y. Atta, B. Y. Jibril, B. O. Aderemi, and S. S. Adefila, *Appl. Clay Sci.* 61, 8 (**2012**).
42. M. M. J. Treacy and J. B. Higgins, Collection of Simulated XRD Powder Patterns for Zeolites (fifth), edited by M. M. J. Treacy and J. B. Higgins, Elsevier Science B.V., Amsterdam (**2007**), pp. 52–53.
43. J. B. Loos, *Zeolites* 18, 278 (**1997**).
44. A. Boultif and D. Louer, *J. Appl. Crystallogr.* 37, 724 (**2004**).
45. M. M. J. Treacy and J. B. Higgins, Collection of Simulated XRD Powder Patterns for Zeolites (fifth), edited by M. M. J. Treacy and J. B. Higgins, Elsevier Science B.V., Amsterdam (**2007**), pp. 278–279.
46. K. S. W. Sing, D. H. Everett, R. A. W. Haul, L. Moscou, R. A. Pierotti, J. Rouquerol, and T. Siemieniewska, *Pure and Applied Chemistry* 57, 603 (**1985**).
47. G. Majano, A. Darwiche, S. Mintova, and V. Valtchev, *Ind. Eng. Chem. Res.* 48, 7084 (**2009**).
48. M. M. Mostafa, K. N. Rao, H. S. Harun, S. N. Basahel, and I. H. A. El-Maksod, *Ceram. Int.* 39, 683 (**2013**).
49. R. M. A. Roque-Malherbe, Adsorption and Diffusion in Nanoporous Materials, CRC Press, Taylor and Francis, Boca Raton (**2007**).
50. F. Rouquerol, J. Rouquerol, and K. Sing, Adsorption by Powders and Porous Solids Principles, Methodology and Applications, Academic Press, London (**1999**).
51. X. Wang, J. C. C. Chan, Y. H. Tseng, and S. Cheng, *Micropor. Mesopor. Mater.* 95, 57 (**2006**).
52. F. Rouquerol, J. Rouquerol, and K. S. W. Sing, Handbook of Porous Materials, Wiley-VCH (**2002**).
53. W. Loewenstein, *Am. Mineral.* 39, 92 (**1954**).
54. D. Freude and J. Haase, NMR Basic Principles and Progress, edited by P. Diehl, E. Fluck, H. Günter, R. Kosfeld, and J. Seelig, Springer-Verlag, Berlin, (**1993**), Vol. 29, pp. 1–90.
55. R. Abalos, E. Erdmann, and H. A. Destéfanis, *Lat. Am. Appl. Res.* 33, 59 (**2003**).
56. J. C. Jansen, F. J. van der Gaag, and H. van Bekkum, *Zeolites* 4, 369 (**1984**).
57. W. Fan, R. Li, J. Ma, B. Fan, and J. Cao, *Microporous Mater.* 4, 301 (**1995**).
58. M. A. Ali, B. Brisdon, and W. J. Thomas, *Applied Catalysis A: General* 252, 149 (**2003**).
59. P. A. Jacobs, H. K. Beyer, and J. Valyon, *Zeolites* 1, 161 (**1981**).
60. G. Coudurier, C. Naccache, and J. C. Vedrine, *J. Chem. Soc., Chem. Commun.* 1413 (**1982**).
61. W. Mozgawa, *J. Mol. Struct.* 596, 129 (**2001**).
62. M. Sitarz, W. Mozgawa, and M. Handke, *J. Mol. Struct.* 404, 193 (**1997**).
63. N. A. S. Amin and D. D. Anggoro, *J. Nat. Gas Chem.* 12, 123 (**2003**).
64. R. Buzzoni, S. Bordiga, G. Ricchiardi, C. Lamberti, A. Zecchina, and G. Bellussi, *Langmuir* 12, 930 (**1996**).
65. K. Sadowska, K. Góra-Marek, and J. Datka, *Vib. Spectrosc.* 63, 418 (**2012**).

ARTICLE